Acta Cryst. (1978). A**34**, 289–296

The Electronic Stationary Picture Method for High-Speed Measurement of Reflection Intensities from Crystals with Large Unit Cells

BY NGUYEN HUU XUONG, STEPHAN T. FREER, RONALD HAMLIN, CHRIS NIELSEN AND WAYNE VERNON

Departments of Biology, Physics and Chemistry, University of California, San Diego, La Jolla, CA 92093, *USA*

(*Received* 18 *July* 1977; *accepted* 17 *October*, 1977)

A method for measuring X-ray intensity data from crystals with large unit cells is presented. The method takes full advantage of the capabilities of the multiwire area detector diffractometer. This diffractometer is a high-speed data collection system utilizing a multiwire proportional chamber that can detect photons from all simultaneously occurring reflections and record the diffraction pattern as a two-dimensional histogram in a computer mass core memory. In the electronic stationary picture method of data collection, reflection intensities are extracted from a sequence of electronic pictures each of which is exposed while the crystal is stationary. Between successive pictures the crystal is rotated about a fixed axis by a small constant angle of approximately 0·05°. Because the integrated intensity of each reflection is extracted from several consecutive pictures, advance prediction of detector coordinates and picture number is required for all reflections and the data-extraction computer program is necessarily complex. Expressions are derived for reflection detector coordinates and setting angles, the system hardware and software are described, the data collection procedure is outlined, and the quality of 7×10^5 reflection intensities measured during six months of operation is analyzed.

Introduction

The structure determination of a macromolecule by X-ray diffraction techniques involves measurement of thousands of reflection intensities from crystals that are likely to deteriorate in the X-ray beam. Since a crystal with 50 Å unit-cell axes, a typical size for a small protein, produces approximately 100 simultaneous reflections, the speed and efficiency of data collection can be maximized only if all these simultaneous intensities are measured at the same time. Collection of reflection intensities from crystals with large unit cells, either with a conventional diffractometer or with film, is very inefficient: the diffractometer has high photon counting efficiency but can measure at the most two or three reflections at a time, while film can record all simultaneously occurring reflections but with low counting efficiency. The advantages of both methods can be realized with an area detector capable of recording electronically, with high counting efficiency, the coordinates of all diffracted photons.

Area detector diffractometers that use an image intensifier together with a TV camera are now being developed in several laboratories (Arndt & Ambrose, 1968; Minor, Milch & Reynolds, 1974; Abrahamsson, 1972; Hashizuma, Kohza & Kinoshita, 1972). In our laboratory we have assembled a data collection system that utilizes a multiwire proportional chamber (Charpak, 1970) and a large high-speed computer core memory. This Multiwire Area Detector (MAD) diffractometer is capable of measuring more than 1000 reflection intensities per hour. The advantages of the multiwire chamber have been outlined and the system hardware has been described previously (Xuong & Vernon, 1972; Cork, Fehr, Hamlin, Vernon, Xuong & Perez-Mendez, 1973, 1974; Cork, Hamlin, Vernon, Xuong & Perez-Mendez, 1975). We here present the Electronic Stationary Picture (ESP) method of data collection, a method that takes full advantage of the capabilities of the MAD diffractometer.

In the ESP method of data collection, reflection intensities are extracted from a sequence of electronic pictures each of which is exposed while the crystal is stationary. Between successive pictures the crystal is rotated about a fixed axis by a small constant angle of approximately 0·05°. This is to be contrasted with standard rotation methods in which the crystal is continuously oscillated by a few degrees during the entire time the detector is recording the diffraction pattern. The ESP method has two principal advantages: First, since all data are measured with the crystal stationary, reflection overlap is minimized or eliminated altogether; second, since intensity data are extracted from a definite x–y location of the detector *only* during the interval when the diffracted beam is actually present, the peak-to-background counting ratio is maximized (in rotating-crystal methods counts are accumulated even when the Bragg conditions are not satisfied). These two advantages are particularly significant for data collection from crystals with large unit cells which produce large numbers of densely packed weak reflections.

In order to be truly practical, the ESP method requires an electronic area detector and a mass core

storage from which the counts for any particular location can be easily and rapidly read out. The ESP method is similar to the step-scanning technique used in conventional diffractometry. Because the integrated intensity of each reflection is extracted from several consecutive pictures, the advance prediction of the location and picture number is required for all reflections and the data-extraction computer program is necessarily complex.

In this paper we derive expressions for the X,Y detector coordinates and the ω setting angle of the reflections, describe the hardware and software of the system, outline the data collection procedure, and analyze the quality of the intensity data measured during routine operation of the system over the last six months.

Diffraction geometry

Consider the general reciprocating lattice point, P. Its position just after the crystal has been lined up on the diffractometer is given in three different coordinate systems by equations (1) through (3):

Crystal system:

$$\overrightarrow{OP} = h\mathbf{a}^* + k\mathbf{b}^* + l\mathbf{c}^*; \tag{1}$$

Machine Cartesian system:

$$\left.\begin{aligned} x &= \lambda(ha_x^* + kb_x^* + lc_x^*) \\ y &= \lambda(ha_y^* + kb_y^* + lc_y^*) \\ z &= \lambda(ha_z^* + kb_z^* + lc_z^*) \end{aligned}\right\}, \tag{2}$$

where a_x^* is the projection of $\mathbf{a}^*$ on the machine Cartesian x axis, *etc.*, and λ is the X-ray wavelength. The x axis coincides with the rotation axis of the crystal. The z axis (normally coincident with the X-ray beam) is perpendicular to the rotation axis and lies in the plane determined by the rotation axis and the X-ray beam; the positive z direction is from the crystal toward the X-ray source. The y axis is mutually perpendicular to the x and z axes.

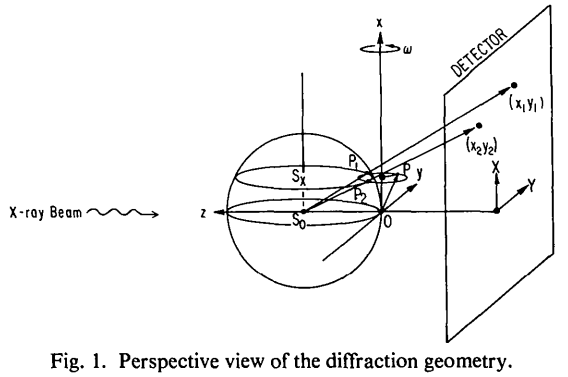

Fig. 1. Perspective view of the diffraction geometry.

Cylindrical coordinate system:

$$\left.\begin{aligned} \zeta &= x \\ \varphi &= \tan^{-1} z/y \\ \xi &= (y^2 + z^2)^{1/2} \end{aligned}\right\}. \tag{3}$$

The experimental set up is shown schematically in Fig. 1, a perspective view of the sphere of reflection, crystal rotation axis, and detector. When the crystal is rotated about the x axis by angles ω_1 and ω_2, P intersects the sphere of reflection at P_1 and P_2 and therefore gives rise to scattered rays S_oP_1 and S_oP_2. The expressions for rotation angles ω_1 and ω_2 can be obtained from Fig. 2(*a*), a section through the sphere of reflection perpendicular to the x axis at height x:

$$\begin{aligned} \omega_1 &= PO_xy + yO_xP_1 = (2\pi - \varphi) + (\pi/2 - \beta) \\ &= \pi/2 - \varphi - \beta, \text{ modulo } 2\pi, \end{aligned} \tag{4}$$

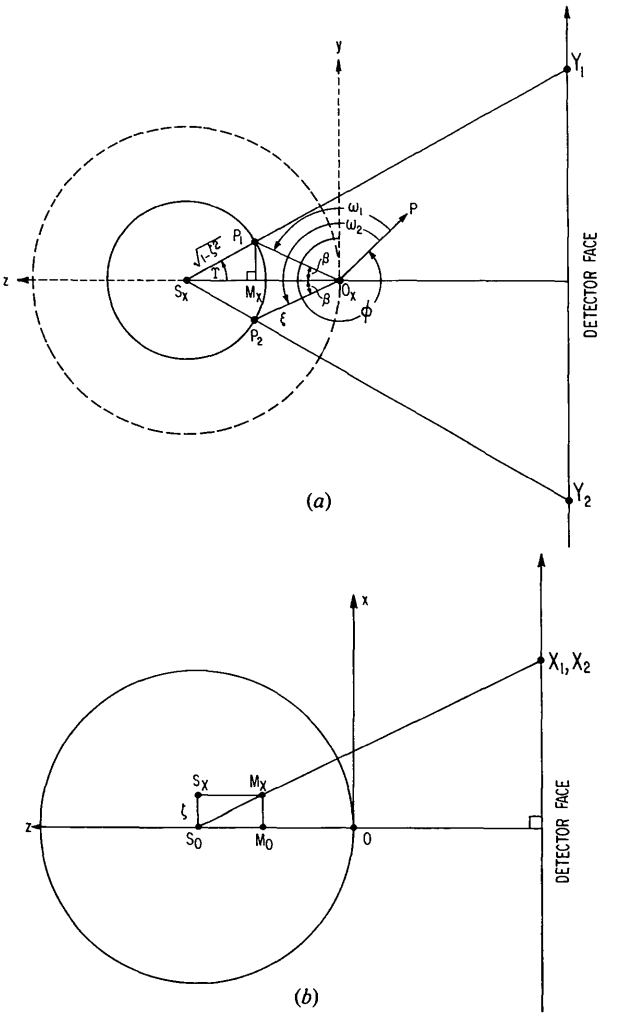

Fig. 2. Sections through the sphere of reflection for normal diffraction geometry. (*a*) Section perpendicular to the x axis at height x, *i.e.* through the diffracting reciprocal lattice points P_1 and P_2. (*b*) Section perpendicular to the y axis at $y = 0$.

$$\omega_2 = \omega_1 + 2\beta = \pi/2 - \varphi + \beta \text{ modulo } 2\pi. \quad (5)$$

The expression for cos β can be obtained with the law of cosines:

$$\cos\beta = (\overline{S_xO_x}^2 + \overline{P_1O_x}^2 - \overline{S_xP_1}^2)/2\,\overline{S_xO_x}\,\overline{P_1O_x}.$$

Substituting the appropriate cylindrical coordinates and noting that $\overline{S_xP_1} = (1-x^2)^{1/2} = (1-\zeta^2)^{1/2}$ from right triangle $S_oS_xP_1$ (Fig. 1), we obtain

$$\cos\beta = \frac{1^2 + \xi^2 - (1-\zeta^2)}{2\xi} = (\xi^2 + \zeta^2)/2\xi. \quad (6)$$

Next we obtain expressions for X_1, Y_1 and X_2, Y_2, the detector coordinates of the scattered rays. These are most conveniently derived from the respective X and Y sections through the sphere of reflection shown in Fig. 2. From the similar triangles in Fig. 2(b) we have:

$$\frac{X_1}{D} = \frac{X_2}{D} = \frac{\overline{M_xM_o}}{\overline{S_oM_o}},$$

where D is the crystal-to-detector distance. Since $\overline{M_xM_o} = \zeta$, and $\overline{S_oM_o} = \overline{S_xM_x} = (1-\zeta^2)^{1/2}\cos\Upsilon$ (Fig. 2a) it follows that

$$X_1 = X_2 = \frac{D\zeta}{(1-\zeta^2)^{1/2}\cos\Upsilon}. \quad (7)$$

From Fig. 2(a) we have

$$\begin{aligned} Y_1 &= D\tan(\Upsilon) \\ Y_2 &= D\tan(-\Upsilon). \end{aligned} \quad (8)$$

The value for Υ can be obtained by applying the law of cosines in triangle $S_xO_xP_1$ of Fig. 2(a).

$$\cos\Upsilon = (\overline{S_xP_1}^2 + \overline{S_xO_x}^2 - \overline{O_xP_1}^2)/2\,\overline{S_xP_1}\,\overline{S_xO_x}$$
$$\cos\Upsilon = (2-\zeta^2-\xi^2)/2(1-\zeta^2)^{1/2}. \quad (9)$$

The above expressions are valid if both the detector face and the crystal rotation axis are perpendicular to the incident beam. If, in order to measure high-order reflections, the detector is rotated by an angle θ_c about the vertical rotation axis, then, as can be seen from the yz section through the sphere of reflection at height x shown in Fig. 3(a), the detector coordinates of diffracted rays OP_1 and OP_2 become

$$X_1 = \frac{\zeta D}{(1-\zeta^2)^{1/2}\cos(\Upsilon - \theta_c)} \quad (10)$$
$$Y_1 = D\tan(\Upsilon - \theta_c) + D\tan\theta_c$$

and

$$X_2 = \frac{\zeta D}{(1-\zeta^2)^{1/2}\cos(-\Upsilon - \theta_c)}$$
$$Y_2 = D\tan(-\Upsilon - \theta_c) + D\tan\theta_c.$$

The xz section remains as in Fig. 2(b) but notice that $\overline{S_xM_x} = (1-\zeta^2)^{1/2}\cos(\Upsilon - \theta_c)$ since point M_x is defined as the projection of P_1 on the chamber normal passing through S_x.

Sometimes, owing either to experimental design or to goniostat misalignment, the rotation axis is tilted so that it deviates from the normal by an angle μ. Then, as can be seen in the xy section through the sphere of reflection at $y = 0$ (Fig. 3b),

$$\overline{S_\mu O_\mu} = \cos\mu$$

and

$$\overline{S_\mu S_x} = \zeta + \sin\mu.$$

Therefore cos β, cos Υ can still be calculated from equations (6) and (9) but with

$$\overline{S_xO_x} = \overline{S_\mu O_\mu} = \cos\mu \quad (11)$$

and

$$\overline{S_xP_1}^2 = 1 - \overline{S_\mu S_x}^2 = 1 - (\zeta + \sin\mu)^2.$$

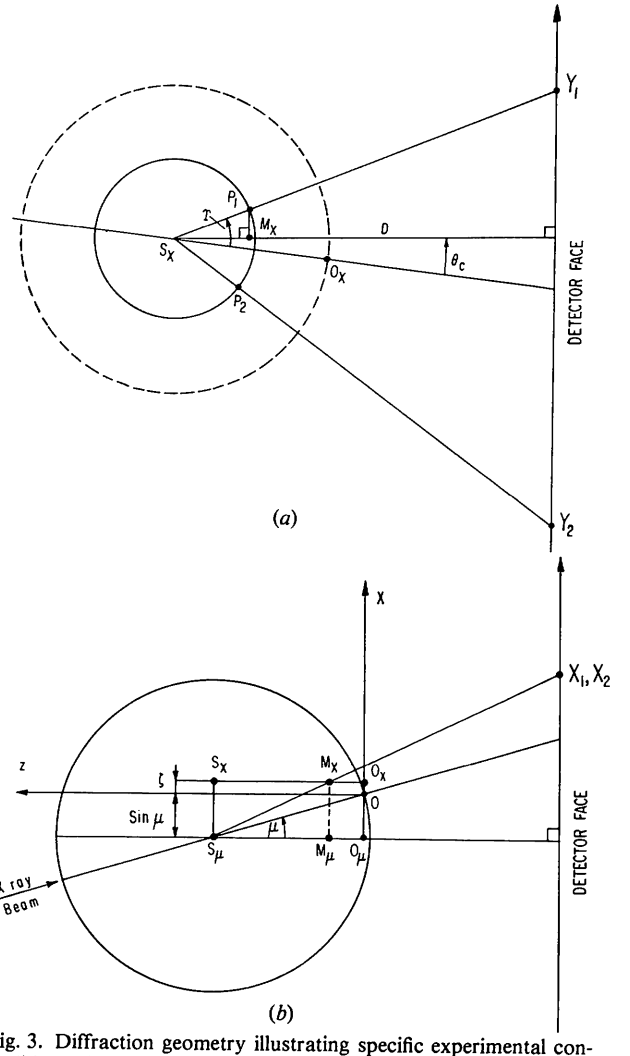

Fig. 3. Diffraction geometry illustrating specific experimental conditions. (a) As in Fig. 2(a), but with the detector rotated by an angle θ_c about the crystal rotation axis. (b) As in Fig. 2(b), but with the X-ray beam inclined at angle μ.

With the above formulas, the general expression for the detector coordinates of diffracted rays OP_1 and OP_2 can be deduced from Fig. 3:

$$X_1 = \frac{(\zeta + \sin\mu)D}{[1-(\zeta+\sin\mu)^2]^{1/2}\cos(+\Upsilon-\theta_c)} - D\tan\mu \qquad (12)$$

$$Y_1 = D\tan(\Upsilon-\theta_c) + D\tan\theta_c$$

and

$$X_2 = \frac{(\zeta + \sin\mu)D}{[1-(\zeta+\sin\mu)^2]^{1/2}\cos(-\Upsilon-\theta_c)} - D\tan\mu \qquad (13)$$

$$Y_2 = D\tan(-\Upsilon-\theta_c) + D\tan\theta_c.$$

The rotation angles for rays OP_1 and OP_2 remain ω_1 and ω_2 as given in equations (4) and (5).

The Lorentz polarization factors can be found in Buerger (1960) with

$$\frac{1}{L} = \cos\mu\sin\Upsilon\,(1-\zeta^2)^{1/2} \qquad (14)$$

and

$$P = 1 + \cos^2 2\theta.$$

The rotation angle, ω, determined above for diffraction of a particular reciprocal lattice point, was derived assuming an infinitesimal crystal and a parallel X-ray beam. In practice the combination of finite crystal size and incident beam divergence cause each reciprocal lattice point to produce a diffracted ray throughout a small range in the rotation angle, $\Delta\omega$. This rotation range has been determined by Phillips (1954) for a divergence angle, α, in the XOZ plane. It is proportional to $\alpha x L$ where x is defined above in equation (2) and L is the Lorentz factor defined in equation (14). If we assume the beam divergence is cylindrically symmetrical about the z axis then we replace x by $(x^2+y^2)^{1/2}$ and get

$$\Delta\omega \approx \alpha L(x^2+y^2)^{1/2}. \qquad (15)$$

This approximation predicts well the angular range of diffraction for reflections from protein crystals to at least 2 Å resolution.

The rotation angle, $\Delta\omega$, varies according to the distance of the reciprocal lattice point from the rotation axis. Obviously a point in diffracting position that lies on the rotation axis will diffract continuously at all values of ω. Thus, reflections with large $\Delta\omega$ should be deleted from the data set since, in general, it is unduly difficult to determine their integrated intensities. Computation considerations, then, dictate the upper limit of $\Delta\omega$.

The beam divergence also produces a slight change, that is a function ω, in the position of the reflection on the detector. We have verified that over the entire range of $\Delta\omega$ for a particular reflection, the change in detector coordinates is less than one raster width of the detector and can therefore be compensated for by the reflection-centering routing described in the next section.

System hardware and software

Hardware

A block diagram of the MAD diffractometer is shown in Fig. 4. The components of the diffractometer have been described previously (Cork *et al.*, 1973, 1974), so their function will be but briefly outlined here. The X-ray source is a Picker ultra-stable X-ray generator with a copper target tube; the crystal is oriented with a GE three-circle goniostat controlled by the META-4 computer with the help of three stepping motors; scattered X-ray photons are detected in the multiwire area detector; the coordinates of each photon are determined by the X,Y-address encoder, and data are stored in the mass core memory as a two-dimensional histogram. The memory is large enough to store two complete pictures, the data picture and its corresponding composite background picture (see below).

The spatial resolution of the 25 × 25 cm chamber is such that it can be divided into 128 × 128 cells. A typical reflection usually covers an area corresponding to a 3 × 3 matrix of these cells. The mass core controller uses the x,y-address of the detected photon to index the appropriate location in the mass core memory which is then incremented by one count. After counts have been accumulated for sufficient time, the diffraction pattern is interpreted by computer program and the contribution to each reflection is stored in a magnetic disk file. For crystal alignment, the entire diffraction pattern can be displayed on the TV monitor through the digital-to-analog converter.

To minimize attenuation of the diffracted rays by air scattering, a helium-filled box is placed between the crystal and the area detector. The box has front and back windows of 0·001 inch mylar and is kept at atmospheric pressure with a continuous flow of helium.

Software

In order to describe the system software meaningfully it is necessary first to outline briefly the data collection procedure of the ESP method. This procedure is very simple. After the crystal is aligned on the

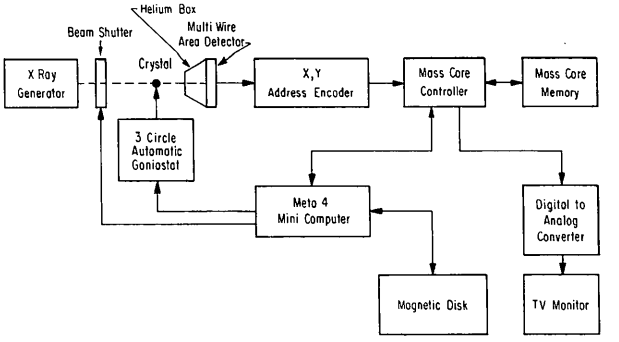

Fig. 4. Block diagram of the multiwire area detector diffractometer.

goniostat and set to a starting orientation, the system cycles through the following three steps:

1. Counts are accumulated from the entire chamber for a preselected time to form a digital picture of the diffraction pattern in the mass core memory.

2. Peak and background contributions to the integrated intensity of each reflection in this picture are estimated and stored in memory.

3. The crystal is rotated by a preselected increment, $\delta\omega$, and the system begins the cycle at step 1 again.

Because steps 2 and 3 require so little time, the beam shutter is left open continuously during the entire data collection period.

The software system is composed of three sets of programs concerned with (1) prediction of detector coordinates and ω setting angles, (2) collection of intensity data, and (3) determination of initial background. There is, in addition, a set of utility programs. The names and functions of these programs are listed in Table 1.

(1) *Prediction programs.* X,Y coordinates and ω setting angles are calculated by program *HFRMG* for all lattice points in the sphere of reflection out to a specified resolution. An ω range is specified, and reflections whose values fall outside this range are discarded. The Lorentz–polarization correction and $\Delta\omega$, the range in rotation angle over which the reciprocal lattice point will remain in reflecting position, are calculated. If $\Delta\omega$ exceeds a specified limit, the reflection is discarded. The ω values for the remaining in-range reflections are rounded to the nearest setting angle $n\delta\omega$, where n is an integer and $\delta\omega$ is the amount by which ω is advanced between consecutive pictures during data collection. The reflections are sorted into frames, which are sets of reflections with the same value of n, and stored on a disk file by programs *XBLCK* and *XCLAS*.

(2) *Data collection program.* During the data collection run, data are continuously streaming out of the chamber and the X,Y-address encoder. However, the computer, through the mass core controller, selects the exposure time during which data are permitted to enter the mass core to form an ESP. The sequence of operations of data collection is controlled by program *DCOLL*. *DCOLL* first sets to zero the contents of all locations in the mass core memory and then opens the gate in the mass core controller for a predetermined time. Next, it sets up the PTABL array for this picture. For each reflection in the picture the array contains the reflection indices, chamber coordinates, LP factor, ω and $\Delta\omega$, and has space reserved for the intensity profile and background estimate. By definition, reflections from groups $n-4$ through $n+4$ are assigned to picture n. After the ESP is formed, the peak and background counts for every reflection in the picture are extracted and stored back in the PTABL array. The computer then advances ω by $\delta\omega$ and the process is repeated.

Peak and background counts of each reflection are determined in the following way: predicted coordinates are obtained from the PTABL array and modified as necessary by the reflection-centering routine. The reflection-centering routine performs a center-of-mass computation from a matrix of 3 by 3 cells centered on point X,Y and can modify X and Y a maximum of ± 1 raster point depending on the location of the center of mass. The peak–background determination subroutine then adds the counts from a 3 by 3 matrix of cells centered on the modified reflection position to obtain the peak value, and estimates the background correction from the corresponding cells in the background picture. The PTABL array is large enough to hold peak-minus-background counts from nine consecutive pictures. These nine measurements form the intensity profile for each reflection from which its integrated intensity is estimated. The Lorentz–polarization correction is applied, and the resulting integrated intensity is stored in a new data file together with its estimated standard deviation.

After the data picture is processed, the background picture is updated. Since the background picture is obtained by summing 16 consecutive pictures, each cell is updated by diminishing its contents by $\frac{1}{16}$ and then adding the contents of the equivalent cell in the data picture. Updating is not done either if the equivalent cell in the data picture was used in the computation of a

Table 1. *Programs for crystal alignment and data extraction from electronic stationary pictures*

Name	Type	Function
HFRMG	Prediction program	Calculate the positions of reflections on the chamber and their ω setting.
XBLCK	Prediction program	Sort the reflections into blocks with same range of ω.
XCLAS	Prediction program	Partition the reflections in each block into frames having the same value of ω.
DCOLL	Data collection program	Rotate crystal, accumulate counts, generate reflection profile, estimate reflection intensity.
BGML	Background program	Generate an initial background picture.
ALIGN	Utility program	Assist operator in aligning crystal.
REFIN	Utility program	Collect rough data for refinement.
PARA7	Utility program	Refine crystal parameters and estimate precise initial crystal orientation.
XSHOT	Utility program	Take a stationary picture at an ω angle and display it together with the prediction from *XCLAS*.
XSORT	Utility program	Sort the reflection output in h,k,l order.
XPNCH	Utility program	Output integrated intensity for all recorded reflections on cards or tape.

reflection intensity or if its contents differ by more than one estimated standard deviation from $\frac{1}{16}$ of the contents of the background cell. Formation of the initial background picture is described in the next section.

(3) *Program to form the initial background picture.* After a starting ω angle has been selected for a data run, program *BGML* is run to set up the initial background picture. *BGML* takes a sequence of 16 pictures near the starting ω angle. For each exposure, the chamber is enabled for a specified time and a data picture formed. Areas associated with predicted reflections are marked, and one of the following background update Fortran equations is used for each cell of the picture.

$$\mathrm{BGND}(i,j) = \mathrm{BGND}(i,j) + \mathrm{DATA}(i,j) \qquad (16)$$

$$\mathrm{BGND}(i,j) = \mathrm{BGND}(i,j) + \frac{1}{N-1}\,\mathrm{BGND}(i,j), \qquad (17)$$

where i and j are the cell coordinates, BGND is the contents of the background cell, DATA is the contents of the data cell, and $N = 1, 2, \ldots, 16$. Equation (16) is the standard update equation, while (17) is used when cell (i,j) falls in a predicted reflection area or DATA(i,j) is abnormally high or low. For the first ESP, *i.e.* for $N = 1$, the program replaces the contents of a cell that occurs in a predicted reflection area by the average of the contents of the surrounding cells. After all 16 pictures are taken, the composite background picture is displayed and the operator is given the option to 'smooth out' portions of it. This is necessary only rarely when spurious peaks occur.

(4) *Utility programs.* This set of programs was written to make data collection as easy and as routine as possible. It is composed of:

(*a*) *ALIGN* which assists the operator in aligning the crystal. The program collects and displays the diffraction pattern, helps the operator estimate crystal misalignment by measuring the center of the zero-level circle with an electronic cursor on the video screen, and then allows the operator to perform any necessary crystal realignment by driving the goniostat stepping motors to newly specified setting angles. If necessary, the program can record and display an oscillation picture which can be used for locating the reciprocal axes.

(*b*) *REFIN* and *PARA7* which collect data on a roughly aligned crystal and refine the unit-cell parameters and setting angles that specify the crystal orientation at the beginning of a data collection run.

(*c*) *XSHOT* which enables the operator to compare an actual picture with the predicted positions of the reflections. After the cell parameters and initial crystal orientation have been refined, the prediction programs (*HFRMG*, *XBLCK* and *XCLAS*) are run. For any specified setting angle, ω, *XSHOT* marks the position of all predicted reflections with crosses superimposed on the display of the diffraction pattern. If all visible reflections are accompanied by a marker, then data collection can be started.

(*d*) *XSORT* and *XPNCH* which are used after completion of a data collection run to sort the reflections in h,k,l order and to output them on punched cards or magnetic tape.

Data collection procedure

In this section the symbols φ, χ and ω designate conventional setting angles for a three-circle goniostat, 2θ is the Bragg angle, and θ_c is the angle between the chamber normal and the incident beam. A data collection 'run' consists of a consecutive series of electronic stationary pictures with ω advanced by a specific amount between each picture and with every picture in the series taken at the same χ and φ setting angles and exposure time.

To correct for radiation damage to the crystal and X-ray absorption, every 'run' is divided into scaling shifts of 100 frames each (about a 5° rotation of ω). There are a sufficient number of symmetry-related reflections in each shift to permit precise determination of the scale constants by least squares. This is the only absorption correction applied and it is analogous to the phi-correction applied to conventional diffractometer data.

The most convenient goniostat setting is with $\chi = 0°$, since at this angle it is possible to avoid obscuring the detector by the χ circle for an entire run by keeping $\omega = 0°$ and stepping along φ. Because it is necessary to discard reflections from reciprocal lattice points that lie near the rotation axis, other runs with different χ settings may be required to obtain a complete set of data.

The crystal-to-detector distance is chosen so that the detector is as close as possible to the crystal without producing overlapping reflections. Since with our present chamber all counts that fall within a 6 × 6 mm area contribute to the intensity of a particular reflection, adjacent reflections should not produce spots closer together than 6 mm. Thus, for a typical crystal with 100 Å unit-cell axes, the crystal-to-detector distance is set at 50 cm. At this distance, the chamber, which has a detection area of 25 × 25 cm, is set at $\theta_c = 20°$ in order to measure data with Bragg spacings from 20 to 2·6 Å. To collect higher or lower resolution data, the chamber may be set at larger or smaller θ_c. The 6 × 6 mm spot size is due both to geometry of the X-ray source and crystal and to properties of the area detector. Improvements in detector design will reduce the spot size to 4 × 4 mm.

The data collection procedure is straightforward. The crystal is mounted on the goniostat and roughly aligned, usually with a principal axis along the X-ray

beam, with the help of program *ALIGN*. A small set of data is collected with program *REFIN* and the unit-cell parameters and initial setting angles are refined by program *PARA7*. For each data collection run, setting angles, detector coordinates, and Lorentz–polarization corrections are computed and sorted for all reflections by programs *HFRMG*, *XBLCK* and *XCLAS*. Predicted setting angles and detector coordinates are checked with *XSHOT* and the initial background picture is generated by program *BGML*. Intensity data are then measured automatically by program *DCOLL*. Operator intervention is required only at the end of the run to output the results and to start the next run.

The system is easy to use and an operator can be trained in less than one week. There have been only about three weeks of down time during the last six months, which is surprisingly low for a new system.

Quality of the data

During the last six months we have measured approximately 7×10^5 reflection intensities on four proteins. The reproducibility of these data are given in Table 2 together with pertinent crystal parameters.

Dihydrofolate reductase from E. coli. For 2·5 Å resolution data we were able to measure in six days approximately 80 000 reflection intensities from 12 000 reflections on one crystal before the average intensity dropped by 15%. With a Hilger and Watts diffractometer it was possible to obtain only 6000 measurements with a crystal of the same size. Reproducibility of the data was the same for both instruments. Intensity measurements were also collected for two heavy-atom derivatives. An electron density map phased on these derivatives was readily interpretable and a model of this protein, with two 17 000 dalton molecules in the asymmetric unit, has been constructed (Matthews, Alden, Bolin, Freer, Hamlin, Xuong, Kraut, Poe, Williams & Hoogsteen, 1977). We now have measured intensities to 1·7 Å resolution on the parent crystal.

Dihydrofolate reductase from L. casei. We have measured 2·5 Å intensity data on the parent and one heavy-atom derivative. An electron density map phased on this single isomorphous replacement is even more easily interpretable than the map from the *E. coli* reductase, and model building is now underway.

Cytochrome c peroxidase. These crystals are frequently twinned and we usually have to mount at least five crystals before finding one of sufficient quality for data collection. Even with these crystals the intensity profiles of reflections in some orientations are fairly broad and sometimes split into two peaks. This probably accounts for the relatively high R_{sym} of 7%. We have measured intensities for the parent protein plus two heavy-atom derivatives and are presently interpreting the resulting electron density map. Unfortunately, we do not know the amino-acid sequence of this protein.

Cytochrome f. We have so far obtained only one crystal of data collection quality for this protein. From it we were able to obtain parent intensity data to 2·5 Å. A Bijvoet-difference Patterson synthesis calculated with this data clearly showed Harker peaks and cross peaks that are consistent with two positions that are presumably the locations of the iron atoms in the two molecules of the asymmetric unit. As yet no heavy-atom derivatives have been found. While searching for derivatives we are attempting to solve the structure with the rotation function from a portion of Cytochrome *c* structure (Takano, Trus, Mandel, Mandel, Kallai, Swanson & Dickerson, 1977).

In summary, we feel the stationary picture method is the optimum procedure for measuring reflection intensity data from crystals with large unit cells. However, since 5000 or more pictures may be exposed for one crystal, it is only practical with an electronic area detector coupled to a mass core storage. Because each stationary picture can contain partial information for 100 or more intensity profiles and the intensity profile of each reflection is obtained from different consecutive pictures, the computer programs are necessarily complex. In routine operation the ESP method has been easy to use and has provided high quality reflection intensity data.

Table 2. *Reproducibility of MAD intensity data*

	Space group	Cell axes (Å)			Number of intensity measurements	R_{sym}* (%)
		a	*b*	*c*		
Dihydrofolate reductase (*E. coli*)	$P6_1$	93	93	73	350 000	4
Dihydrofolate reductase (*L. casei*)	$P6_1$	72	72	93	130 000	5
Cytochrome *c* peroxidase	$P2_12_12_1$	107	51	77	180 000	7
Cytochrome *f*	$I222$	87	70	66	30 000	5

$$*R_{sym} = \frac{\sum_{hkl} \sum_{i=1}^{N} |\langle I(h,k,l)\rangle - I(h,k,l)_i|}{\sum_{hkl} \sum_{i=1}^{N} I(h,k,l)_i}$$ where the inner summation is over all measurements of symmetry-related reflections.

This project was funded by grants from the National Science Foundation (PCM 74-18676) and from the National Institutes of Health (GM 20102, RR 00757 and a career development award (STF) GM 70-140-3).

References

ABRAHAMSSON, S. (1972). *Acta Cryst.* A**28**, S248.
ARNDT, U. & AMBROSE, B. K. (1968). *IEEE Trans. Nucl. Sci.* **NS15:N63**, 92–94.
BUERGER, M. J. (1960). *Crystal-Structure Analysis*. New York: John Wiley.
CHARPAK, G. (1970). *Ann. Rev. Nucl. Sci.* **20**, 195–253.
CORK, C., FEHR, D., HAMLIN, R., VERNON, W., XUONG, N. H. & PEREZ-MENDEZ, V. (1973). *Proceedings of the Int. Conf. on Computers in Chemical Education, Ljubljana-Zagreb.*
CORK, C., FEHR, D., HAMLIN, R., VERNON, W., XUONG, N. H. & PEREZ-MENDEZ, V. (1974) *J. Appl. Cryst.* **7**, 319–323.
CORK, C., HAMLIN, R., VERNON, W., XUONG, NG H. & PEREZ-MENDEZ, V. (1975). *Acta Cryst.* A**31**, 702–703.
HASHIZUMA, H., KOHZA, K. & KINOSHITA, K. (1972). *Acta Cryst.* A**28**, S249.
MATTHEWS, D., ALDEN, R. A., BOLIN, J. T., FREER, S. T., HAMLIN, R., XUONG, N., KRAUT, J., POE, M., WILLIAMS, M. & HOOGSTEEN, K. (1977). *Science*, **197**, 452–455.
MINOR, T. C., MILCH, J. R. & REYNOLDS, G. T. (1974). *J. Appl. Cryst.* **7**, 323–333.
PHILLIPS, D. C. (1954). *Acta Cryst.* **7**, 746–751.
TAKANO, T., TRUS, B. T., MANDEL, N., MANDEL, G., KALLAI, O. B., SWANSON, R. & DICKERSON, R. E. (1977). *J. Biol. Chem.* **252**, 759–775.
XUONG, NG. H. & VERNON, W. (1972). ACA Meeting, Albuquerque, Abstract J10.

Acta Cryst. (1974). A**34**, 296–308

Investigation of Thin MoO_3 Crystals by Convergent-Beam Electron Diffraction

BY L. A. BURSILL*, W. C. T. DOWELL, P. GOODMAN & N. TATE

Division of Chemical Physics, CSIRO, PO Box 160, *Clayton, Victoria, Australia* 3168

(*Received* 11 *July* 1977; *accepted* 19 *October* 1977)

The MoO_3 structure is analysed by means of multi-slice calculations for crystals up to 80 Å thick. It is shown that for such thin crystals convergent-beam patterns can be simply analysed. This allows crystal thickness to be readily determined and opens up the way to more precise structure factor measurements. Many-beam calculations are also used to analyse unit-cell and symmetry data obtained by convergent-beam diffraction/microscopy observations of '101' domains in molybdenum trioxide, showing that $[MoO_6]$ octahedra in domains are more nearly regular than in MoO_3. This is supported by analysis of thermal diffuse scattering. The '101' domain structure has space group *Cmcm* and unit-cell parameters identical to those of the molybdenum oxide–hydroxide $Mo_4O_{10}(OH)_2$. A qualitative comparison of calculated and observed intensities for the space-group-forbidden 100 reflexions of MoO_3 indicates the presence of epitaxically deposited surface layers. This observation, together with the evidence of a hydroxylated domain structure, suggests that thin crystals are formed with epitaxic hydroxyl layers which diffuse into the bulk structure when the crystals are heated.

Introduction

Platelet crystals of MoO_3 were formed by burning Mo in air and subsequently collecting the oxide on a thin carbon film. These crystals offer almost ideal test specimens for thin-crystal convergent-beam diffraction. The initial aim of the present investigation was to show which parameters can be conveniently or accurately measured from crystals of only a few unit cells thick. This work could subsequently be continued with a view to obtaining accurate structure factors, since initial calculations have shown thin-crystal data to be relatively free of absorption effects. Work presented here is restricted to making use of the initial and less accurate data, which may nevertheless be usefully interpreted by means of *N*-beam calculations.

Three types of diffraction pattern are used:

(1) Focused convergent-beam diffraction patterns obtained with the source focused on the crystal and giving patterns characteristic of one region. The same patterns in over-exposure allow observation of the thermal-diffuse-scattering (TDS) pattern.

(2) Defocused convergent-beam patterns obtained with the source focused below the crystal. These give

* Permanent address: Department of Physics, Melbourne University, Parkville, Australia.